ABSTRACT

RAMAN SCATTERING IN FREE STANDING POROUS Si FILMS

by
Thenappan Chidambaram

In this thesis, Raman Scattering of free standing porous silicon on sapphire samples of controllably varying porosity is studied. The free standing, fully crystalline porous silicon films were prepared by electrochemical etching and the porous structure were lifted-off by a procedure based on electro-polishing. During Raman scattering measurements, the samples are exposed to relatively high intensity laser radiation. Free-standing porous Si sample temperature and thermal conductivity are calculated by comparing intensities of Stokes and anti-Stokes Raman peaks. Compared to crystalline Si, we find strong decrease in thermal conductivity accompanied by a change in the phonon spectra. Also, comparing Stokes and anti-Stokes Raman spectra, we find that porous Si is a nano-composite material with a complex morphology and variety of crystallites sizes. The porous silicon layers can be used for thermal isolation and as floating substrates for lattice-mismatched hetero-integration.

RAMAN SCATTERING IN FREE STANDING POROUS Si FILMS

by
Thenappan Chidambaram

A Thesis
Submitted to the Faculty of
New Jersey Institute of Technology
in Partial Fulfillment of the Requirements for the Degree of
Master of Science in Electrical Engineering

Department of Electrical and Computer Engineering

May 2008

APPROVAL PAGE

Raman scattering in free standing porous silicon films

Thenappan Chidambaram

March 31, 2008

Dr. Leonid Tsybeskov, Thesis Advisor — Date
Professor of Electrical and Computer Engineering, NJIT

03/31/2008

Dr. Hussein I. Hanafi, Committee Member — Date
Adjunct Professor of Electrical and Computer Engineering, NJIT

03/31/2008

Dr. Marek Sosnowski, Committee Member — Date
Professor of Electrical and Computer Engineering, NJIT

BIOGRAPHICAL SKETCH

Author: Thenappan Chidambaram

Degree: Master of Science

Date: May 2008

Undergraduate and Graduate Education:

- Master of Science in Electrical Engineering,
  New Jersey Institute of Technology, Newark, NJ, 2008

- Bachelor of Science in Electrical Engineering,
  BITS, Pilani, India, 2004

Major: Electrical Engineering

To my Parents

ACKNOWLEDGMENT

I would like to express my deepest appreciation to Dr. Leonid Tsybeskov, who not only served as my research supervisor, providing valuable and countless resources, insight, and intuition, but also constantly gave me support, encouragement, and reassurance. Special thanks are given to Dr. Hussein I. Hanafi, and Dr. Marek Sosnowski for taking time and being part of the committee.

Many of my fellow research students in the Laboratory are deserving of recognition for their support. I sincerely thank Sandy for helping me with the experiment and simulation. I also wish to thank Lee and Nikhil for their assistance over the months.

TABLE OF CONTENTS

LIST OF FIGURES

LIST OF TABLES

CHAPTER 1

INTRODUCTION

Porous silicon is quickly becoming an increasingly important and versatile nanocomposite material in today's micro- and nano-fabrication technology. Its reactive porous nature allows for the selective formation of unique electronic components and mechanical nanostructures. By controllably varying the etching parameters during the fabrication of porous silicon structures, the porous films can be made to emit light in the spectral range extending from ultra-violet to infra-red. This property enabled porous structures to be used in photonics. The low temperature oxidation of porous silicon has already been utilized in electronic isolation technology and fabrication of embedded silicon-on-insulator (SOI) devices. Due to large surface area of pores they can also be used as a sacrificial layer in surface micromachining. PS has a low thermal conductivity which allows it to be used as a new Si-based thermal insulator because of its compatibility with standard silicon-based technologies.

The most common fabrication technique for the formation of porous silicon (PS) is electrochemical etching of a crystalline silicon wafer in a hydrofluoric (HF) acid-based solution. The electrochemical process allows for precise control of the properties of PS such as thickness of the porous layer, porosity, and average pore diameter. Depending on the etching parameters, for example current density, HF concentration, or substrate doping type and level, the physical properties of PS can be varied [1]

Many theories on the formation mechanisms of PS have been reported since its discovery. One of the theories put forward state that the material in the PS is depleted of carriers and the presence of a depletion layer is responsible for current localization at

pore tips where the field is intensified [2]. Another one describes the morphology of PS based on the hypothesis that the rate of pore growth is limited by the diffusion of holes to the growing pore tip [3] [4].

My contribution towards this thesis was in calculation of temperature of free standing porous silicon on sapphire substrates from the stokes and anti-stokes intensities obtained from Raman scattering measurements using U1000 double monochromator spectrometer and calculation of thermal conductivity of the sample.

The objectives of this thesis are:

1. By studying the published data on porous Si fabrication, optimize the electrochemical etching conditions in the order to obtain the required porosity and pore morphology.

2. Fabricate porous silicon by electrochemical etching in HF-based solution using a heavily doped p-type crystalline Si substrate with an epitaxial layer of intrinsic silicon.

3. Optimize the lift-off procedure for a thin (< 1 um) porous Si film by applying a step-like voltage pulse without damaging the film.

4. Analyze physical properties of porous Si free-standing film, mainly via Raman scattering measurements. Optimize Raman scattering measurements by using proper laser wavelength, power, size of the focused spot, etc.

5. Perform Stokes and anti-Stokes Raman measurements, calculate temperature of free-standing porous Si films with different porosities and determine their thermal conductivity. Explain the obtained results by comparison with thermal conductivity of different solid state materials (e.g., crystalline and amorphous Si, amorphous SiO2, SiGe alloys and superlattices).

CHAPTER 2

POROUS SILICON

2.1 Porous Silicon - Morphology

Pore geometry refers to the diameters of pores and distances between pores. Pore morphology addresses the pore shape (e.g., cylindrical, branched). Pores are classified into micro, meso and macro pores. Pores with dimensions of < 2 nm are classified as micro pores, pores with dimensions between 2nm and 50 nm are termed meso pores and pores with dimensions > 50 nm are termed macro pores (Table 2.1) [5]. The term 'nanopores' is not used in the strict sense and it loosely refers to pore dimensions well below 1 μm.

Table 2.1 Pore size classification

Type of porous Si	Corresponding size regime for dominant porosity (nm)
Microporous	≤2
Mesoporous	2–50
Macroporous	>50

The microporous regime is dominated by quantum size effects. Meso- and macroporous silicon formation is dominated by space charge effects. The different pore size regimes and their dependence on the substrate resistivity are illustrated in Figure 2.1

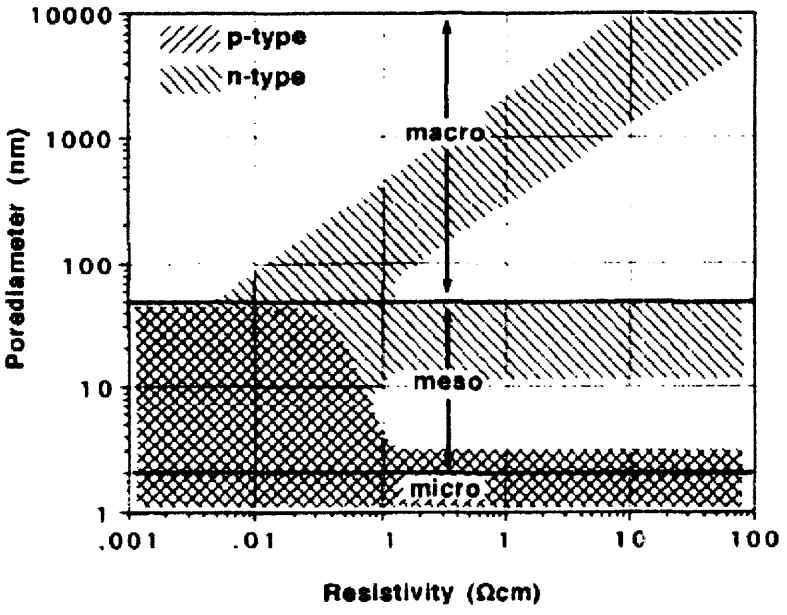

Figure 2.1 The three pore sizes which form on n-type and p-type silicon substrates during anodization in hydrofluoric acid are shown as a function of the substrate resistivity.

The overall structure of porous Si layers depends very strongly upon anodization conditions and the resistivity (magnitude and type) of the Si itself. Pore diameters and spacings can vary over a very wide range from the nanometer scale up to the micron scale. It has been demonstrated that when anodized p^+ Si is examined using x-ray diffraction, the atomic lattice is dilated with respect to the substrate and that the expansion increases with increasing porosity. Low temperature annealing experiments have shown[6] that the dilation of the lattice may be induced by hydrogen bonded to the exposed internal surfaces, while oxide formed on aged porous Si may introduce stresses which yield a similar lattice expansion[7][8].

The structure of p^+ porous Si is strongly anisotropic and the pores with long voids run perpendicular to the surface. TEM imaging of the mesoporous structure is shown in Figure 2.2.

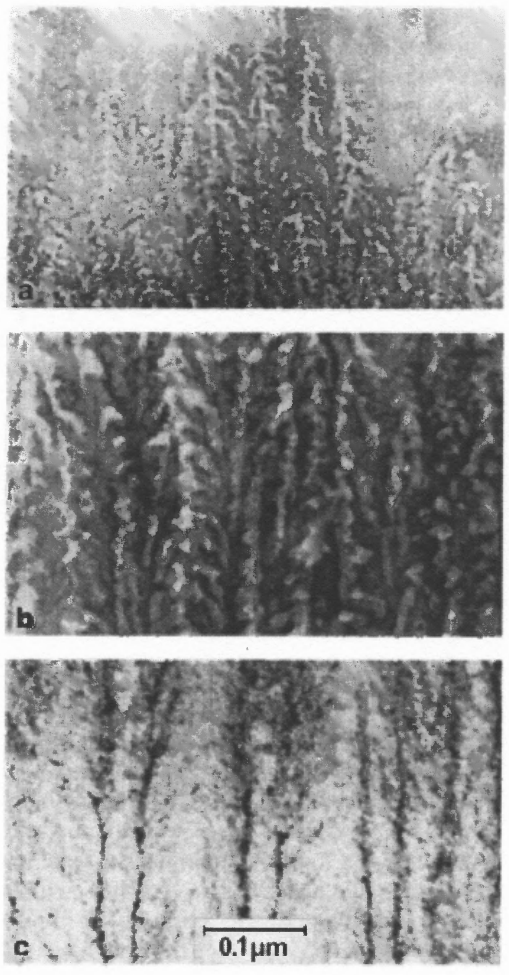

Figure 2.2 TEM cross-sectional images of mesoporous structure formed by anodising p^+ Si: (a) 31% porosity, (b) 51% porosity, and (c) 79% porosity [9].

Figure 2.2 shows (001) p^+ Si anodized over a range of conditions to give porosities of from 31% to 79%. It is clear that long pores lie along the <001> direction perpendicular to the Si surface and have widths in a range around 10 nm. The pores themselves are heavily branched and exhibit a very characteristic ''fir tree'' configuration. For the highest porosity material, the pores are relatively indistinct. But all porous layers are found to be fundamentally crystalline.

2.2 Formation of Porous Silicon

Porous silicon is formed on a silicon substrate during anodization in an hydrofluoric electrolyte. Pore formation is only observed for current densities below a critical current density J_{PSL}. Generally porosification is obtained by anodizing the semiconductor in a suitable electrolyte under suitable conditions. The parameters that are needed to be considered are electrolyte chemistry, applied potential or current density, temperature, flow conditions of the electrolyte, doping type and level of the semiconductor and surface conditions(polished, rough). The necessary chemical reaction at the semiconductor-electrolyte interface is generally a mixture of direct dissolution, oxide formation and oxide dissolution. The silicon-oxide complex formed is an intermediate complex which gets dissolved in the solution. During pore formation, direct dissolution of the semiconductor almost always competes with oxidation plus subsequent dissolution of the oxide. HF dissolves the oxide that is formed during the chemical reaction. Another prerequisite for the dissolution reaction is the presence of electronic holes. In general, at least one hole is needed to initiate the reaction chain at the interface that ultimately leads to the loss of one atom. The equation of the overall process during the PS formation can be expressed as follows:

$$Si + 2HF + 2h^+ \rightarrow SiF_2 + 2H^+$$

$$SiF_2 + 4HF \rightarrow H_2 + H_2SiF_6$$

The etching rate is determined by the holes (h^+) accumulation in the adjacent regions of the HF electrolyte and Si atoms. In the case of p-type material it is necessary to drive the system in a state where holes can only be consumed at certain places. By using a highly

doped semiconductor most of the voltage is dropped on the electrolyte side of the junction and it leads to a fast chemical reaction favouring direct dissolution in comparison to anodic oxidation.

The reaction mechanism is anisotropic i.e. etching rate on each crystallographic plane is different. Anisotropic silicon etching is a key technology for the fabrication of micromechanical devices. It allows for the precise three-dimensional structuring of miniature sensors and actuators in an IC compatible way. The central feature of all anisotropic etchants is the slow etch rate of the (111) crystal planes, being approximately one to two orders of magnitude smaller than for other principal crystal orientations. (111) surface atoms possess only one dangling bond, whereas there are two for all other main crystal surfaces.

Standard mesopores in Si are always grown on heavily doped samples and at relatively high HF concentrations, which necessitates only a few volts to drive large etching currents. The solid - liquid junction of Silicon and HF - containing liquids exhibits a number of peculiar features, e.g. a very low density of surface states. If the junction is biased, the I-V characteristics in diluted HF are quite complicated and exhibits two current peaks and strong current or voltage oscillations at large current densities (Figure 2.3).

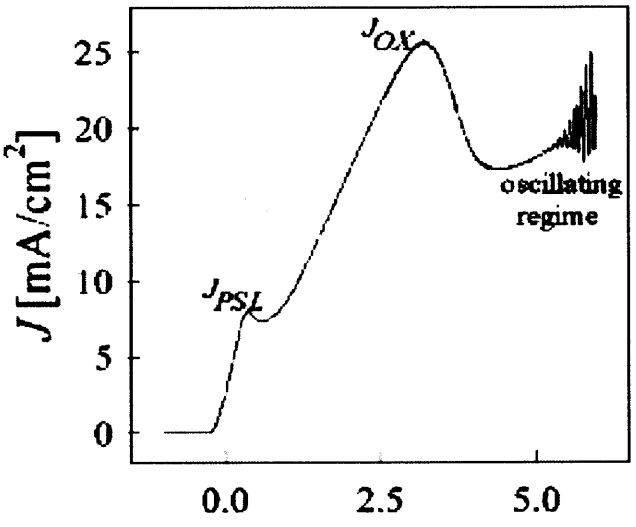

Figure 2.3 The I-V characteristics of the silicon- hydrofluoric acid contact shows different phenomena from generation of a porous silicon layer (PSL), oxidation and electropolishing (OX) and electrochemical oscillations at higher anodic bias.

These oscillations have been described quantitatively by the Current-Burst-Model. The Current Burst Model states that the dissolution mainly takes place on small spots in short events, starting with a direct Si dissolution, and possibly followed by an oxidizing reaction. After these two short processes, the oxide hump undergoes dissolution, a time-consuming process which ensures at the location of the current burst a dead-time of fixed length during which no new burst can start. However, immediately after dissolution the Si surface has the highest reactivity, resulting in a maximal probability of another current burst. Due to H-termination the surface becomes passivated, and the probability for bursts decays until it reaches the properties of a completely passivated Si surface, comparable to the situation before the nucleation of the first Current Burst.

While at high current densities the semiconductor surface is completely covered with oxide, at low current densities, most of the semiconductor surface will be in direct contact to the electrolyte. It is well known [1] that after chemical dissolution the free surface is passivated, i.e. the density of surface states decreases as a function of time which increases the stability of the surface against further electrochemical attack. For silicon, the speed and the perfection of passivation of the (111) crystallographic surface is larger than for the (100) surface. This selective aging of surfaces leads to a self amplifying dissolution of (100) surfaces (which will become pore tips) and a preferential passivation of (111) surfaces (which will become pore walls). Under optimized chemical conditions with an extremely large passivation difference between (111) and (100) surfaces a self organized growth of octahedral cavities occurs.

The well established model by Lehmann et al. [10] explains the micro-pore formation as a consequence of a charge transfer across the Si/electrolyte interface. Depending on the pore tip geometry this current is dominated by carrier diffusion rather than thermionic emission or tunneling of holes. This results in the continuous advance of the dissolution at the pore tip. The passivation of the pore sidewall results from the depletion of holes in the space charge region (SCR) between two neighbouring pores if their distance decreases to two times the SCR.

Porosity (P) can be calculated from the weights of unetched specimen (m1), just after electrochemical etching (m2) and after removal of the whole porous layer (m3).

The corresponding equation is

$$P = \frac{m1-m2}{m1-m3}$$

The growth of pores is controlled by many factors, such as:

– type of silicon (n, p: determines pore size and etching conditions),

– wafer orientation ((100) is etched about 50 times faster than (111)),

– wafer finishing (polished one or both sides and surface roughness),

– doping level (usually in the range 1014–1019 atoms/cm3; with increased doping decreasing pore size),

– masking technology (determines growth direction and trench size),

– H-termination treatment before electrochemical etching (cleaning procedure, resulting in reduction of surface state),

– HF concentration (2–50 wt%: increased HF results in higher current density),

– ethanol concentration (it is an active surface agent: removes hydrogen bubbles during etching, reduces surface tension; layers have higher porosity),

– current density (anodic 1–100 mA/cm2; higher current results in faster etching),

– time (from seconds to hours; longer time results in thicker layer),

– intensity and direction of illumination (topside, backside or without illumination of the wafer; illumination generates holes, necessary for silicon dissolution; illumination is not necessary in the case of p-type or highly doped n-type silicon),

– electrochemical cell construction (single or double cell: double cell is used on a large-scale fabrication),

– volume of the cell (larger volume of the electrolyte is more accurate for homogeneous

etching),

– purging of the electrolyte (nitrogen removes free oxygen and suppresses oxidation),

– mixing of the electrolyte (removes bubbles of hydrogen),

– temperature (should be constant).

2.3 Effect of Etching Parameters on Pore Geometry

Doping has an effect on the porosity and diameter of micropores. The porosity and pore depth of porous structures grown on polished Si wafers with resistivities varying between 6 and 1000 ohm-cm in HF at 23°C is shown in Table 2.2. The current is fixed at 5.5 mA/cm^2 [12]

Table 2.2 Porosity and pore depth with varying substrate doping

Resistivity (ohm-cm)	Surface porosity (%)	Pore depth (μm)
6	**72**	**17.5**
10	**58**	**19**
23	**44**	**32.2**
1000	**28**	**53**

It is evident that the porosity decreases with increasing resistivity. Also the pore depth increases with increasing resistivity. This is due to the fact that the amount of etched Si has to be constant while being operated in galvanostic conditions. In wafers with low resistivity i.e. high doping the distance between two pores is very small due to reduced SCR.

Now, if the current density is changed unlike the case above, the kinetics at the Si/electrolyte interface changes. The porosity and pore diameter, however, do not change with increasing current densities. The pore diameter and etch rate of 20 ohm cm Si wafers etched for 90 min at room temperature with different current densities is shown in Table 2.3 [12].

Table 2.3 Pore diameter and etch rate of a 20 ohm-cm Si wafer at varying current densities.

Current Density (mA/cm^2)	Pore Diameter (μm)	Etch Rate (μm/h)
3	3.4	6
5	3.2	14
10	3.5	36
30	3.4	63
50	Pores do not form	Sample electropolishes

It is seen that at $50mA/cm^2$, there is no pore formation as the sample gets electropolished at such high current densities to give a rough but rather flat surface.

Patterning of the substrate prior to the initial pore growth plays a crucial role on the resulting pore geometry. This method is used for the fabrication of ordered micro-pores in the silicon substrate by anodic etching. The initial position of the pores is defined by lithography. Initially an oxide layer is deposited on the front surface and patterned. Now this oxide layer serves as a mask for subsequent etching to produce small pits on the Si-surface. Due to the anisotropic nature of etching small inverted pyramids with squared

bases are formed. The depth of these pits varies depending on the structure size of the patterning lithography mask. Now the pre-patterned surface enforces the initial pores to grow at the tip of the inverted pyramids. If the resistivity of the sample is high enough, no random pores will grow between these patterned structures. Figure 2.4 shows the pore growth on n-sample where pore positions are predetermined by lithography. It is evident that regular arrays of deep holes are produced.

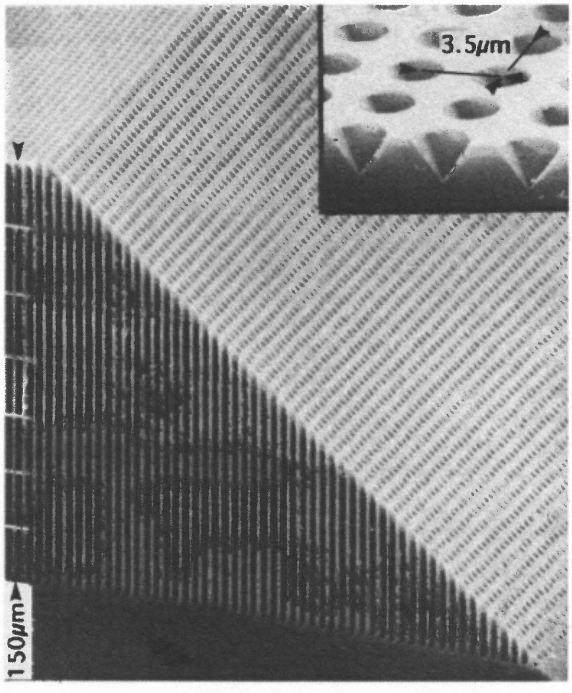

Figure 2.4 Cross-section of an aligned macropore array formed from lithographically-defined initial pits in *n*-Si [13].

The pore geometry is dependent on the concentration of the electrolyte. For the experimental results that follow, the porous structure was prepared by electrochemical anodic etching of a highly doped *p*-type <100> oriented silicon substrate with a resistivity of 0.01–0.02Ωcm. The sample was treated with two different electrolytic concentrations. One with 4 : 6 HF and ethanol by volume and the other with 6 : 4 HF and ethanol by volume In both solutions, concentrations of hydrofluoric acid ethanol were

48% and 98% respectively (Table 2.4). It can be seen that the pore diameter and porosity decreases with increase in HF concentration. For highly doped *p*-type Si, both the pore diameter and wall thickness are largely determined by the thickness of the space-charge layer formed at the interface of electrolyte and Si. Thus, in general, pore diameter has the same order of magnitude as the thickness of the space-charge layer. The wall thickness is generally less than twice the space-charge layer thickness. This is because overlapping of the two space charge regions of neighboring pore walls depletes the carriers and thus makes them not conductive. If the wall thickness is larger than twice the space-charge layer thickness, the walls are not depleted of carriers and dissolution can still occurs to form new pores on the walls [14].

Table 2.4 Variations of pore diameter, porosity, and specific surface area of PS with electrolyte composition at constant current density of 12.5mA/cm^2 [14]

HF	Ethanol	Pore dia. (nm)	Porosity(%)	Specific surface area
4	6	10	50	500
6	4	6	40	710

For *p*-Si, increasing HF concentration reduces the thickness of the space-charge layer and increases the pore tip current density, which results in smaller pores and thicker wall. On the other hand, polishing of silicon in aqueous HF solution is known to be preceded by silicon oxide formation. The oxide is then dissolved by HF through formation of a fluoride complex in the solution. The dissolution rate of silicon oxide increases with increasing HF, which in turn increases the critical current density at which the surface is covered by oxide. As a result, the pores become smaller and walls become thicker with increasing HF concentration. [15] [16]

Figure 2.5 shows the variation of PS layer thickness and porosity with etching time at constant current density of 12.5mA/cm^2

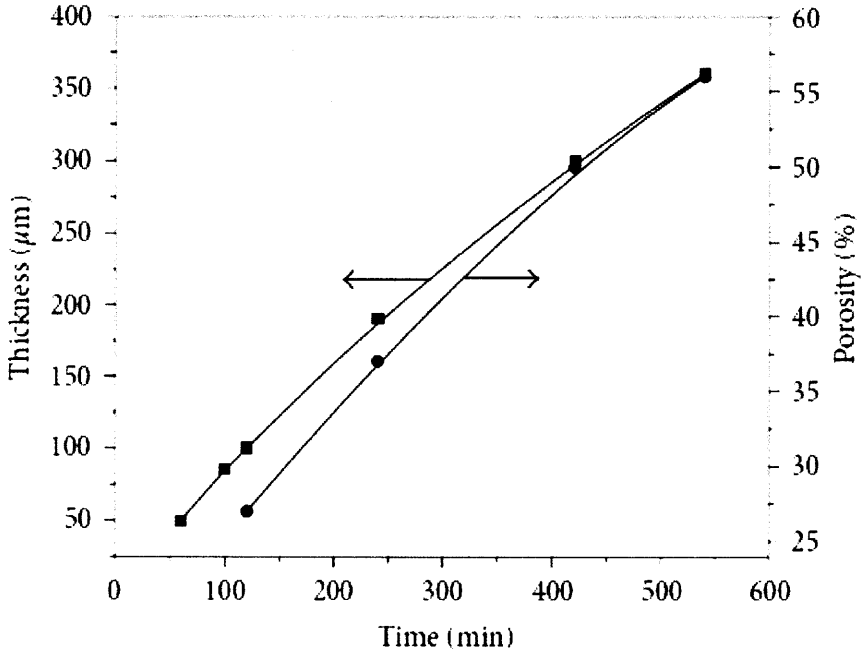

Figure 2.5 Variation of porous layer thickness and porosity with etching time at constant applied current density of 12.5mA/cm^2 [14]

This variation in porosity with thickness is related to the chemical dissolution of the porous material during formation. During the electrochemical reaction, and as a function of the anodizing time, the effect of the chemical dissolution is to increase the average porosity and pore radii.

When PS was etched for one hour at different current densities, it was found that the thickness of PS layer was linearly varying with the applied current density as shown in Figure 2.6.

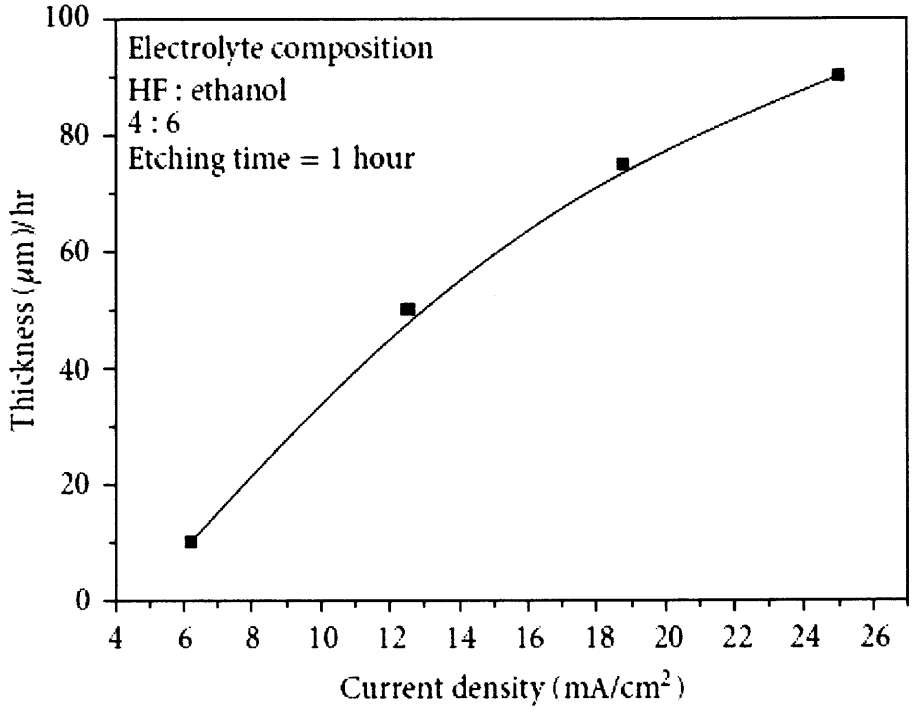

Figure 2.6 Variation of porous layer thickness with different constants applied current density for 1 hour. [14]

2.4 Preparation of Porous Silicon Samples

Porous silicon samples used in this work were prepared by electrochemical anodization process carried out in a single Teflon cell, which is schematically drawn in figure 2.7. The Teflon container pressed the front surface of the Si on wafer through an O-ring(not shown in figure). Backside of silicon wafer is in contact with an Al plate, though which voltage is applied. Crystalline silicon wafer is the anode and a Pt wire is the cathode. Uniform electric field was maintained at the silicon anode surface to obtain uniform thickness and structure of PS Layer. Anodization under galvanostatic conditions is generally the preferred approach for reproducibly attaining wide ranges of porosity and thickness. Careful design of the electrochemical cell is required to achieve good lateral

film uniformity. Layer microstructure is sensitive to many parameters which need to be controlled during etching. These include not only electrolyte composition, current density and applied potential but also electrolyte temperature [17] if excellent reproducibility from run to run is to be achieved.

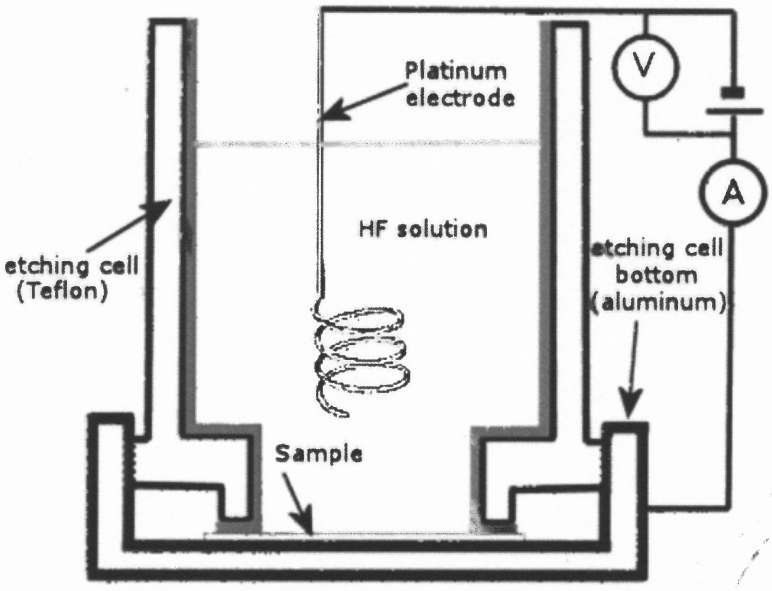

Figure 2.7 Diagram of electrochemical etching cell used for preparation of PS samples. [18]

The etching solution (electrolyte) is prepared by mixing HF, H_2O and C_2H_5OH with volume fractions between 1:1:1 and 1:1:5. Ethanol is most widely used as a surfactant in the case of PS formation. It is added frequently to the hydrofluoric acid to minimize hydrogen bubble formation during anodization and thereby improve layer uniformity [19]. The metal contact was made at the back side of the wafer and sealed so that only the front side of the wafer was exposed to the etching solution. The back side of any semiconductor specimen needs an ohmic contact that ideally covers the whole back side, and has a uniform but small contact resistance. The more important requirement is

uniformity because a not-so-small contact resistance, as long as it is uniform, can always be compensated by a higher voltage.

Free standing porous silicon films of thickness ~0.1 μm to ~100 μm are produced by electrochemical etching and are subsequently lifted off the silicon wafer by an electropolishing step. During electropolishing, the silicon atoms are removed layer by layer and the porous silicon films are separated from the wafer. In electropolishing mode, the current density is increased to about 300 mA/cm^2. The thin films were deposited on sapphire windows where they remain attached by van der Waals or electrostatic forces [24]. The uniform thickness and high surface quality of the films suggest that more than one free-standing film can be produced from the same substrate surface. In obtaining more than one film, only the etching time is changed. There is some increase in surface roughness from the first film to the subsequent films, but the quality of all the films remains high. The increase in roughness is due to the fact that every lifted layer leaves its fingerprint behind on the substrate surface, which acts as the new front surface for the next layer, leading to additional surface inhomogeneities for subsequent layers.

An atomic force microscope (AFM) is utilized to quantify the surface morphology. In AFM, a tip is in contact with the surface and thus the image represents the surface topography (Figure 2.8(a)).

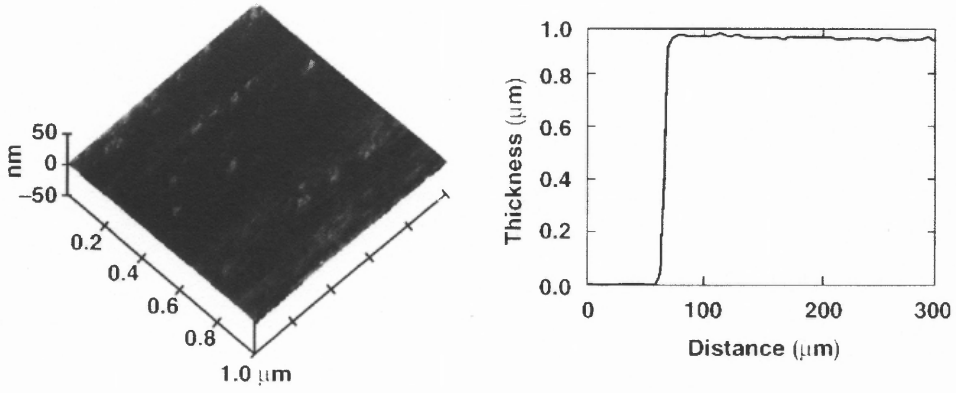

(a) **(b)**

Figure 2.8 (a) AFM image and **(b)** profilometer scan of the free-standing porous film The surface is flat and uniform even on the nanometer scale, indicating that the

crystallites are much smaller than 100 nm. Figure 2.8 (b) shows the thickness of the same sample measured with a profilometer. The principle is similar to the AFM measurement, but it can be conveniently used over much longer distances. We find that the thickness of the porous film remains nearly constant over the entire film diameter. In the transmission spectra of the sample, the modulations are due to Fabry-Perot fringes which are induced by interference between light reflected from the front and back surfaces (Figure 2.9)

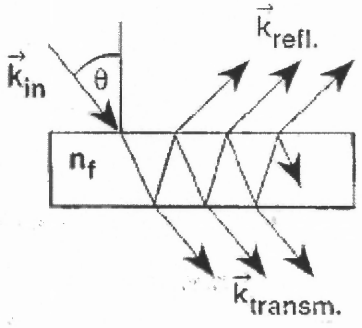

Figure 2.9 Multiple internal reflections from the front and back side of porous films

CHAPTER 3

RAMAN SCATTERING

3.1 Raman Scattering - Overview

When light is scattered from a material system most photons are elastically scattered i.e. the scattered photons have the same frequency and, hence, wavelength, as the incident photons. But a very small portion of the light is scattered at frequencies lower or higher than the incident photon. Such a process is called inelastic scattering or Raman Effect. In classical terms, the interaction can be viewed as a perturbation of the molecule's electric field. In quantum mechanics the scattering is described as an excitation to a virtual state lower in energy than a real electronic transition. Raman Scattering is inherently incoherent and the intensity of scattering is proportional to the number of molecules present in the material system and is independent of its structure. Raman scattering can occur with a change in vibrational, rotational or electronic energy of a molecule. In this report the term Raman Effect implicitly means vibrational Raman Effect only.

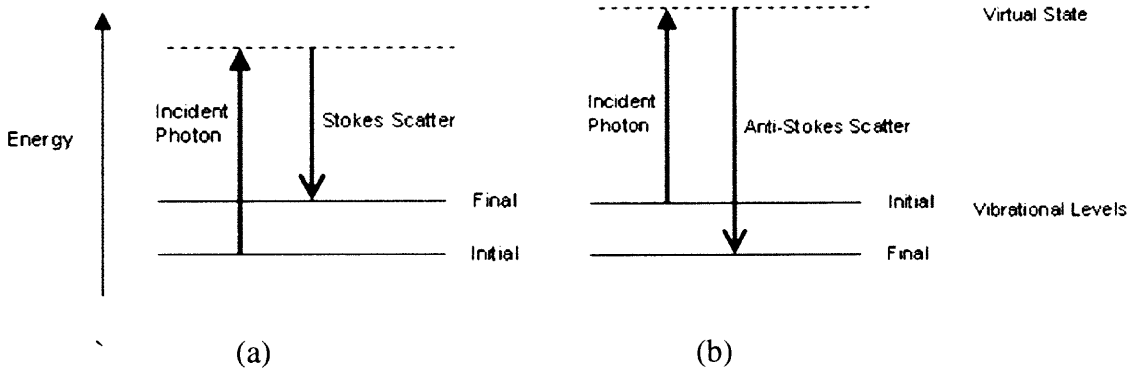

Figure 3.1 Energy level diagram for Raman scattering; (a) Stokes Raman scattering (b) anti-Stokes Raman scattering.

The energy difference between the initial and final vibrational levels, $\bar{\nu}$, or Raman shift in wave numbers (cm^{-1}), is calculated from

$$Raman\ shift = \bar{\nu} = \frac{1}{\lambda_{incident}} - \frac{1}{\lambda_{scattered}}$$

where $\lambda_{incident}$ and $\lambda_{scattered}$ are the wavelengths (in cm) of the incident and Raman scattered photons, respectively. The magnitude of the shift is independent of the excitation frequency. The vibrational energy is dissipated as heat. Because of the low intensity of Raman scattering, the heat dissipation does not cause a measurable temperature rise in a material. At room temperature the thermal population of vibrational excited states is low. Therefore, a large number of atoms are present in the ground state i.e. their initial state is the ground state, and the scattered photon will have lower energy (longer wavelength) than the exciting photon. This is Stokes shift in Raman spectroscopy. Figure 3.1(a) depicts Raman Stokes scattering. A small fraction of the molecules are in vibrationally excited states. Raman scattering from vibrationally excited molecules leaves the molecule in the ground state i.e. final state. The scattered photon appears at higher energy, as shown in Figure 3.1(b). This anti-Stokes-shifted Raman spectrum is always weaker than the Stokes-shifted spectrum. The Stokes and anti-Stokes spectra contain the same frequency information. The ratio of anti-Stokes to Stokes intensity at any vibrational frequency is a measure of temperature. Anti-Stokes Raman scattering is used for contactless thermometry. The anti-Stokes spectrum is also used when the Stokes spectrum is not directly observable, for example because of poor detector response or spectrograph efficiency.

3.2 Raman Selection Rules and Intensities

The dipole moment, **P**, induced in a molecule by an external electric field, **E**, is proportional to the field.

$$\mathbf{P} = \alpha \mathbf{E}$$

where α is the polarizability of the molecule.

The polarizability measures the ease with which the electron cloud around a molecule can be distorted. The induced dipole emits or scatters light at the optical frequency of the incident light wave. Raman scattering occurs because a molecular vibration can change the polarizability. The Raman selection rule is given by

$$\mathbf{d}\,\alpha / \mathbf{dQ} \neq \mathbf{0}$$

where Q is the normal coordinate of the vibration

If a vibration does not greatly change the polarizability, then the polarizability derivative will be near zero, and the intensity of the Raman band will be low. Scattering intensity is proportional to the square of the induced dipole moment, that is to the square of the polarizability derivative $(\mathbf{d}\,\alpha / \mathbf{dQ})^2$

3.3 Raman Instrumentation

The Raman U1000 is a high resolution double spectrometer (with double additive monochromator). This instrument is used in application which demand high spectral resolution (CCD and PMT detection) and high stray light rejection (single channel PMT detection).

A spectrometer is an apparatus designed to measure the distribution of radiation of a source in a particular wavelength region. Its principal components are a monochromator and a radiant power detector such as a photoemissive cell or a photomultiplier tube. Radiant power enters the entrance slit of the monochromator. The monochromator selects a narrow spectral band of radiant power and transmits it through the exit slit to the photosensitive surface of the detector.

A spectrometer consists of the following elements:

1. An entrance slit or aperture stop.
2. A collimating element to make the rays parallel which pass though one point of the entrance slit or field-stop. This collimator may be a lens, a mirror or an integral part of the dispersing element, as in a concave grating spectrometer.
3. A dispersing element, usually a grating which spreads the light intensity in space as a function of wavelength.
4. A focusing element to form an image of the entrance slit or field-stop at some convenient focal plane. The image is formed at the exit slit of a monochromator and at the detector focal plane of a spectrograph.

5. An exit at the focal plane which transmits the light from the image that the focusing system has formed. Usually, this consists of a long narrow slit but there does not need to be a real aperture. The exit field-stop could be, and sometimes is, defined by the detector. In fact, the multichannel system can be designed so that the sensitive area of the detector forms the field-stop.

The Raman U1000 double additive monochromator has been designed for maximum versatility and adaptability to advancing detector technology. It uses standard and blazed holographic plane gratings to ensure optimal throughput in any spectral region.

U 1000 double monochromator spectrometer's ooptical design consists of

- Double additive monochromator
- Asymmetrical Czerny-Turner configuration
- Interchangeable gratings for UV, visible, and IR
- High precision sine drive
- Horizontal axis of grating rotation
- 3 stages / 4 horizontal slits for very low stray light level

Specification of Jobin-Yvon U1000 double monochromator spectrometer is listed in Table 3.1

Table 3.1 Specification of Jobin-Yvon U1000 double monochromator spectrometer

Model	Focal Length	F Nbr	Wavelength Range	Resolution	Dispersion
U 1000	1000 mm	f/8.0	185nm - 40μm	0.004 nm	0.4 nm/mm

Figure 3.2 shows U1000 High Resolution Double Grating Research Raman Spectrometer which consists of a laser, a monochromator and a detection system.

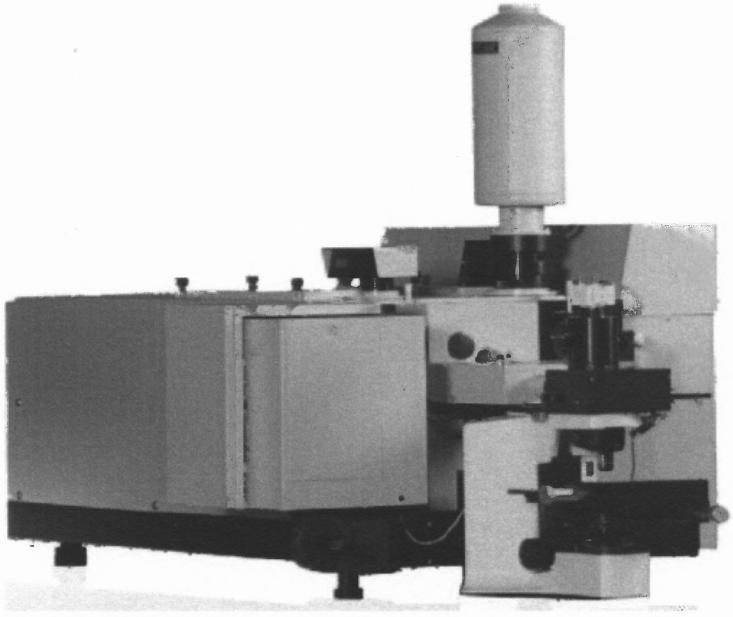

Figure 3.2 U1000 High Resolution Double Grating Research Raman Spectrometer

Laser: A laser is used to excite Raman spectra because it gives a coherent beam of monochromatic light. This gives sufficient intensity to produce a useful amount of Raman scatter and allows for clean spectra, free of extraneous bands.

Monochromator: A monochromator is an optical device that transmits a mechanically selectable narrow band of wavelengths of light chosen from a wider range of wavelengths available at the input. Two monochromators can be used either in subtractive mode to provide a wide field to the spectrograph or in additive mode when higher resolution is required. The double monochromator has one or two slits in between the first and second stage monochromators.

Detection system The detection system includes a multichannel detector (a linear diode array) and a photomultiplier connected to a single photon counter.

Raman spectra are obtained by irradiating the sample with a laser source of visible or near-infrared monochromatic radiation. The choice of the laser depends on the sample material. Generally an Ar ion laser with output wavelengths in the green and blue region, or a Ar-Kr laser with an additional wavelength in the red region is used. The following diagram illustrates a basic Raman scattering setup. The laser is focused orthogonally on a given sample where the incident light scatters. The scattered light is then measured via liquid cooled photomultiplier connected to a computer system The Raman spectrum displayed by the computer system is a plot of the intensity of the Raman scattered radiation as a function of its frequency difference from the incident radiation. The difference in frequency is the Raman shift and is measured in units of cm^{-1}. Since this is a difference value, the Raman shift is independent of the incident radiation.

Raman spectroscopy is an invaluable tool in the investigation of low energy excitations in various materials as well as in the characterization of their electronic, vibrational and structural properties. Strain relaxes selection rules and mixes different phonon modes, and therefore can instantly be recognized through a deviation from the theoretically predicted angular polarization dependence of the Raman intensity [20] [21].

Raman spectra were measured at room temperature with the sample surface inclined at an angle to the incident light. Si–Si polarization Raman measurements were performed at excitation wavelengths of 457.9nm with a power of 300 mW. The scattered light was analyzed using a JY-double monochromator equipped with a cooled

photomultiplier and a photon counting system. Figure 3.3 illustrates the stokes and anti-stokes peaks of three different samples of free standing porous silicon on sapphire. It is evident from the plots that there is about 2 cm^{-1} shift from the Si-Si peak which is indicative of the tensile strain present at the interface between the substrate and porous silicon.

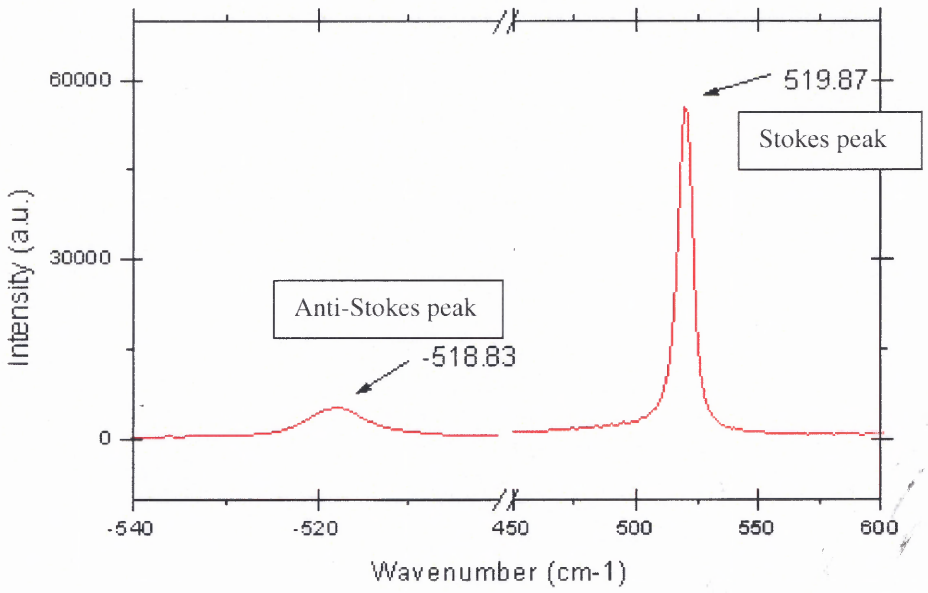

(a)

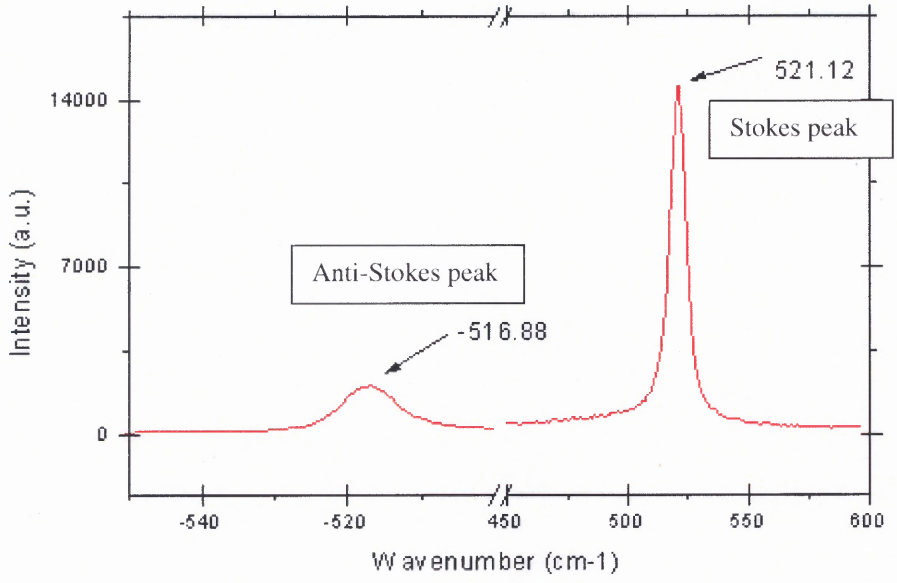

(b)

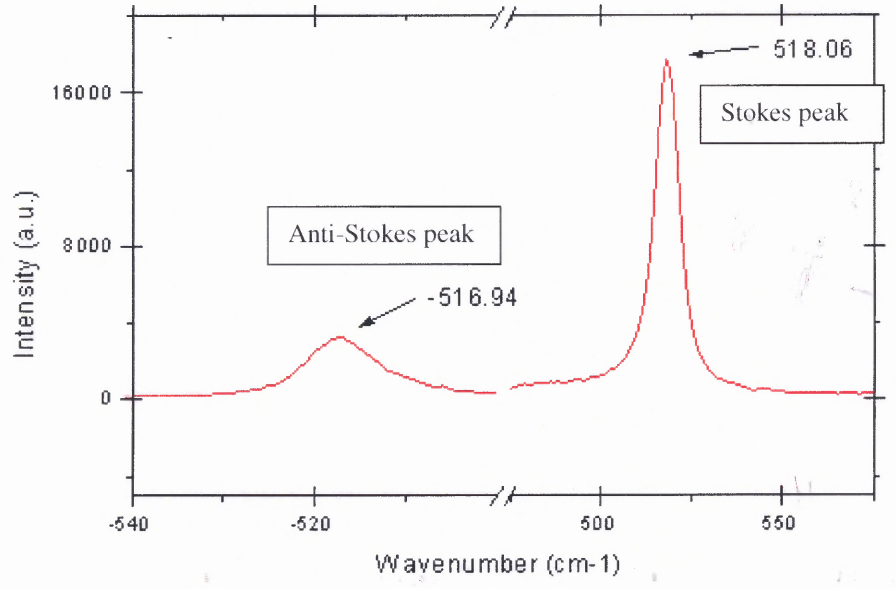

(c)

Figure 3.3 Stokes and Anti-Stokes peaks of three samples are shown in (a), (b) and (c) respectively.

The ratio of the Stokes and Anti-Stokes intensity is a measure of the temperature of the sample. The temperature of the three sample were calculated using the equation

$$e^{(-h\,c\,v\,/\,kT)} = I_{as} / I_s$$

where h (Plank's constant) = 4.135 E-15 eVs

c (speed of light) =3 E10 cm s^{-1}

v (Raman frequency or shift) in cm^{-1}

k (Boltzmann's constant)= 8.6E-5 eV/K

T (Temperature) in K

I_{as} = Anti Stoke intensity @ v

I_s = Stoke intensity @ v

The temperature of the samples in (a), (b) and (c) were found to be 312.7 K, 373.28 K and 434.35 K respectively.

3.4 Thermal Conductivity Calculation

Thermal conductivity, k, is the property of a material that indicates its ability to conduct heat. The thermal conductivity(TC) of Porous silicon (~5 W/mK) is two or three order lower than that of monocrystalline Si(>l00 W/mK). Heat conduction in PS based on phonon diffusion mechanism [22]. They increase with increasing the wafer doping level and with decreasing the porosity of the layers. The extremely low thermal conductivity values can be attributed to three parameters

(i) Porosity

(ii) Nano-scale size of Si crystallites

(iii) Disordered arrangement of the crystallites interconnection

Since TC of Si crystallites is higher than TC of air pores, heat transfer in porous structures occurs only through the crystallites. Interconnections between the Si nanocrystallites play an important role in the heat transport control. Strictly speaking, the notion of TC for a nano- crystallite cannot be introduced because its mean dimension value is smaller than the phonon mean free path in bulk Si (~40 nm) [23]. When the mean free path in monocrystalline is less than the phonon mean free path, there is no phonon scattering inside the crystallites and consequently neither temperature gradient nor notions of TC can be defined. Phonons scatter only at the crystallites boundaries which restore local thermodynamic equilibrium. Therefore only at boundaries, the notion of temperature can be introduced. Between two opposite boundaries the phonon transport has a ballistic nature.

Heat conduction is given by the formula

$$H = \frac{\Delta Q}{\Delta t} = k \times A \times \frac{\Delta T}{x}$$

where $\Delta Q/\Delta t$ is rate of heat flow
k is thermal conductivity
A is the total surface area of conducting surface
ΔT is the temperature difference and
x is the thickness of the conducting surface separating the two temperatures

Rearranging the above equation we get,

$$k = \frac{\Delta Q}{\Delta t} \times \frac{1}{A} \times \frac{x}{\Delta T}$$

In other words,TC is defined as the quantity of heat, ΔQ, transmitted during time Δt through a thickness x, in a direction normal to a surface of area A, due to a temperature difference ΔT, under steady state conditions and when the heat transfer is dependent only on the temperature gradient.

Table 3.2 gives a comparison of the thermal conductivities in the various forms of Si at room temperature (300 K).

Table 3.2 Thermal conductivity of various semiconductor material systems

Semiconductor Material System	Thermal Conducivity (W m^{-1} K^{-1})
c-Si (crystalline silicon)	**130 - 150**
PS (porous silicon)	**5.0 – 15.0**
$Si_{0.5}Ge_{0.5}$ SLs (silicon- germanium superlattices)	**3.0 - 5.0**
SiO_2 (Silicon dioxide)	**1.0 – 1.5**
a-Si (amorphous silicon)	**0.1 - 5.0**

By finding the same surface temperature in c-Si and P-Si, thermal conductivity k becomes directly proportional to Q (heat, assuming it's directly related to power) and x (penetration depth). The penetration depth in c-Si and PS is 600nm and 300m respectively.

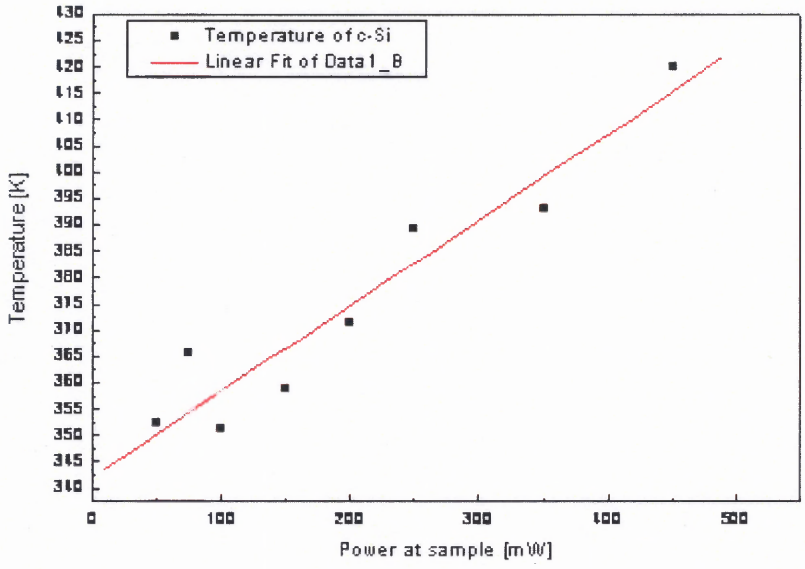

Figure 3.4 Temperature and Power correlation

For one of the PS sample, the temperature was previously found out to be 374K (with 30mW excitation). From Figure 3.4, 374K corresponds to ~200mW. Using the above equation the value of TC for PS turns out to be 13.3 W/m-K. Similarly for the sample with temperature 434K, the TC is 7.27 W/m-K.

In solids, thermal energy is transported by phonon propagation, i.e. via crystal lattice vibration. From a wide variety of phonons, acoustic phonons, mainly due to their nearly linear energy-momentum dependence and the nature of vibrations, are responsible for heat transport. Thus, thermal conductivity (TC), or ability of the lattice to dissipate heat, strongly depends on lattice imperfections (defects), impurities, grain boundaries and interfaces with significant mismatch of the acoustic impedance (i.e. density and sound velocity). Compared to other Si-based solids, high purity single crystal Si has the highest thermal conductivity (second to diamond), while amorphous Si, SiO_2 and SiGe superlattices exhibit almost 100 times lower heat conductance (Table 3.2). The thermal

conductivity of PS free-standing films is found to be 10-100 times lower compared to that of crystalline silicon. Several factors contribute to the found reduction of porous Si thermal conductivity, mainly the structure of this sponge-like nano-material (see TEM pictures). Interestingly, porous Si thermal conductivity is better than that in amorphous Si, most likely due to crystalline nature of the remaining Si structure.

CHAPTER 4

CONCLUSION AND FUTURE WORK

PS is obtained by electrochemical anodization of bulk Si in HF-based solutions. By varying HF concentration and current density during anodization, well defined thin layers with different porosities can be obtained. Raman measurements from free standing porous silicon on sapphire crystal with a (100) crystallographic orientation confirms the presence of a strain field at the interface between the porous silicon and sapphire substrate. The thermal properties of PS strongly depend on the physical parameters of PS films which are strongly dependent upon the fabrication controlling parameters such as electrolyte composition, current density, etching time. The thermal conductivity of PS is very low as compared to Si substrate. This thermal property of porous silicon enables it to be used as a good thermal insulator in semiconductor technology.

REFERENCES

[1] R.Herino, G. Bomchil, K. Barla, C. Bertrand, and J. L. Ginoux, Journal of the Electrochemical Society, vol. 134, no. 8, pp. 1994–2000, 1987.

[2] M. I. J. Beale, J. D. Benjamin, M. J. Uren, N. G. Chew, and A.G. Cullis, Journal of Crystal Growth, vol. 73, no. 3, pp. 622–636, 1985.

[3] R. L. Smith and S. D. Collins, Journal of Applied Physics, vol. 71, no. 8, pp. R1–R22,1992.

[4] R. L. Smith, S. F. Chuang, and S. D. Collins, Journal of Electronic Materials, vol. 17, no. 6, pp. 533–541, 1988.

[5] A.G. Cullis, L.T. Canham, P.D.J. Calcott, J. Apppl. Physics 82(3), 1 August 1997.

[6] H. Sugiyama and O. Nittono, J. Cryst. Growth 103, 156, 1990.

[7] I. M. Young, M. I. J. Beale, and J. D. Benjamin, Appl. Phys. Lett. 46,1133 ,1985.

[8] D. Buttard, D. Bellet, and G. Dolino, J. Appl. Phys. 79, 8060, 1996.

[9] I. J. Beale, J. D. Benjamin, M. J. Uren, N. G. Chew, and A. G. Cullis, J. Cryst. Growth 73, 622, 1985.

[10] V.Lehmann, S.Ronnebeck, Journal of the Electrochemical Society, 146(1999) p. 2968.

[11] Monuko du Plessis, Physica Status Solidi (a) Volume 204, Issue 7 , Pages 2319 – 2328.

[12] Konle, J., Presting, H., Konig, U., Starkov, V., Vyatkin, A.,Nanodevices and nanosystems: specialized applications, 26-28 Aug. 2002 Page(s):457 – 460.

[13] V. Lehmann, J. Electrochem. Soc. 140, 2836, 1993.

[14] Pushpendra Kumar and Patrick Huber, Journal of Nanomaterials, Vol. 2007, Article ID 89718, 4 pages.

[15] X. G. Zhang, Journal of the Electrochemical Society, vol. 151, no. 1, pp. C69–C80, 2004.

[16] H. Foll, J. Carstensen, and S. Frey, Journal of Nanomaterials, vol. 2006, Article ID 91635, 10 pages, 2006.

[17] H. Ono, H. Gomyu, H. Morisalci, S. Nozaki, Y. Shou, M. Shimasaki, M.

Iwase, and T. Izumi, J. Electrochem. Soc. 140, L180, 1993.

[18] M. Balarin , O. Gamulin , M. Ivanda , V. Djerek , O. Celan , S. Music , M. Ristic , K. Furic, Journal of Molecular Structure 834–836 (2007) 465–470.

[19] K. Barla, G. Bomchil, R. Herino, J. C. Pfister, and J. Baruchel, J. Cryst. Growth 68, 721, 1984.

[20] H. Rho, H. E. Jackson, and B. L. Weiss, J. Appl. Phys. 90, 276, 2001.

[21] F. Cerdeira, C. J. Buchenauer, F. H. Pollak, and M. Cardona, Phys. Rev. B 5, 580, 1972.

[22] V. Lysenko, S. Perichon, B. Remaki, and D. Barbier, Journal of Applied Physics Vol.86, No. 12.

[23] J.D. Chung , M. Kaviany, Intern. J. Heat Mass Trans. 43 (2000) 521.

[24] J. von Behren, L. Tsybeskov, and P. M. Fauchet, Appl. Phys. Lett. **66** (13), 27 March 1995.